Milillo, P., Rignot, E., Mouginot, J., Scheuchl, B., Morlighem, M., Li, X., Salzer, J. T. (2017): On the Short-term Grounding Zone Dynamics of Pine Island Glacier, West Antarctica, Observed With COSMO-SkyMed Interferometric Data. - *Geophysical Research Letters*, *44*, 20, pp. 10,436—10,444.

DOI: http://doi.org/10.1002/2017GL074320

AGU PUBLICATIONS

Geophysical Research Letters

RESEARCH LETTER
10.1002/2017GL074320

Key Points:
- We observe significant sort-term grounding line dynamics of a major glacier in west Antarctica
- Faster retreat along shallow bed slopes helps validate bed topography models
- Short-term dynamics implies the presence of a soft bed, a high sensitivity to tides, and flushing of seawater within the grounding zone

Supporting Information:
- Supporting Information S1
- Data Set S1

Correspondence to:
P. Milillo,
pietro0milillo@gmail.com

Citation:
Milillo, P., Rignot, E., Mouginot, J., Scheuchl, B., Morlighem, M., Li, X., & Salzer, J. T. (2017). On the short-term grounding zone dynamics of Pine Island Glacier, West Antarctica, observed with COSMO-SkyMed interferometric data. *Geophysical Research Letters, 44*, 10,436–10,444. https://doi.org/10.1002/2017GL074320

Received 28 MAY 2017
Accepted 27 AUG 2017
Accepted article online 31 AUG 2017
Published online 21 OCT 2017

On the Short-term Grounding Zone Dynamics of Pine Island Glacier, West Antarctica, Observed With COSMO-SkyMed Interferometric Data

Pietro Milillo[1], Eric Rignot[1,2], Jeremie Mouginot[2], Bernd Scheuchl[2], Mathieu Morlighem[2], Xin Li[2], and Jacqueline T. Salzer[3]

[1]Jet Propulsion Laboratory, California Institute of Technology, Pasadena, CA, USA, [2]Department of Earth System Science, University of California, Irvine, CA, USA, [3]Physics of Earthquakes and Volcanoes, GFZ German Research Centre for Geosciences, Potsdam, Germany

Abstract Using radar satellite data from the Italian COSMO-SkyMed (CSK) constellation and the German TanDEM-X formation, we present comprehensive measurements of the biweekly grounding line dynamics of Pine Island Glacier, West Antarctica, from August to December 2015. The 1 day repeat cycle of CSK reveals tidally induced, grounding line migration on the scale of kilometers and extensive seawater intrusion within the grounding zone, which significantly exceeds that predicted for a stiff bed but are consistent with that calculated for a deformable bed. The deformable bed also explains the continuous draining/filling of subglacial lakes proximal to the grounding line. After correction for oceanic tides, we estimate a retreat rate for 2011–2015 of 0.3 km/yr at the glacier center and 0.5 km/yr on the sides, which is 3 times slower than for 1994–2011 (1.2 km/yr at the center). We attribute the decrease in retreat rate to colder ocean conditions in 2012–2013 relative to 2000–2011.

Plain Language Summary Using short-term repeat satellite data from the Italian CSK constellation, we document significant tidal migration of the junction between ice and the ocean on the Pine Island Glacier, West Antarctica, which is the largest contributor to sea level rise from Antarctica. The results imply that the junction is not fixed but corresponds to a zone several kilometers wide where ocean water melts ice from below. At present, numerical models of ice flow do not account for a flush zone. The existence of a flush zone should make the glacier more prone to retreat in response to warmer ocean waters.

1. Introduction

Pine Island Glacier (PIG) is one of the most dynamic ice streams in Antarctica. PIG accounts for 20% of the total ice discharge from the West Antarctic Ice Sheet (WAIS) (e.g., Rignot et al., 2008). PIG has undergone a rapid increase in mass loss, ice thinning, and grounding line retreat over the past 38 years (Park et al., 2013; Rignot, 1998, 2008; Rignot et al., 2008, 2014; Shepherd et al., 2001, 2002; Shepherd & Peacock, 2003). Surface velocities sped up by 50% in 2000–2014 alone (Han et al., 2016; Mouginot et al., 2014) and 75% since the 1970s. Grounding line retreat has proceeded at 1.2 km/yr since 1994 based on observations separated by several years, leaving much uncertainty about the dynamics of the grounding line on shorter time scales (Park et al., 2013; Rignot et al., 2014). This retreat has been fueled by the enhanced intrusion of warm, salty, subsurface ocean water of circumpolar deep water origin onto the continental shelf, beneath the floating ice shelf, to reach the glacier grounding zone and melt it from below (e.g., Dutrieux et al., 2014). The retreat rate is expected to vary depending on the amount of ice melt by the ocean, the rate of ice thinning, the shape of the glacier surface and bed topography, and the departure from hydrostatic equilibrium of ice near the grounding zone. Significant uncertainties remain in the mapping of the bed topography beneath PIG (Rignot et al., 2014) and on the variability of ocean conditions beneath the ice shelf (Jenkins, 2016).

Grounding line mapping is challenging to perform in areas of rapid flow (Scheuchl et al., 2016), here 4 km/yr at the glacier center, because the differential interferometric synthetic aperture radar (DInSAR) signal decorrelates in zones of phase aliasing, i.e., where the glacier displacement rate becomes large enough that the change in interferometric phase per resolution cell is greater than one 360° cycle, so that the interferometric coherence of the phase is lost. The last grounding line position for PIG was obtained in fall 2011 when the European Remote Sensing satellite (ERS-2) was placed in a 3 day repeat mode toward the end of its

mission (Rignot et al., 2014). Existing interferometric synthetic aperture radar (InSAR) instruments do not provide a sufficiently short revisit interval (Sentinel-1a/b is 6 to 12 days, RADARSAT-2 is 24 days, ALOS PALSAR is 14 days, and TerraSAR-X, 11 days) to map the grounding line position since 2011. The only instrument with a repeat pass short enough to enable grounding line mapping is the Italian Space Agency's (ASI's) COSMO-SkyMed (CSK) constellation in a 1 day repeat configuration.

Here we study the biweekly grounding line variability of PIG by exploiting the synergy of the short repeat time of the CSK InSAR combined with precision digital elevation model (DEM) mapping with TanDEM-X (TDX). This unique data set is used to reveal the landward extent of the grounding zone, tidally induced grounding line variability, and the long-term trend in grounding line migration. We discuss our methodology, the observations of grounding line migration with CSK, and their implications for the long-term evolution of PIG.

2. Data and Methods

We tasked CSK SAR acquisitions of PIG to cover its entire grounding zone. CSK consists of a constellation of four low Earth orbit satellites each carrying an X band SAR antenna (3.1 cm wavelength) enabling a finer resolution (3 m) and better sampling rate (up to 176.25 MHz) of ground displacements compared with longer wavelength systems (e.g., 6 cm for C band and 24 cm for L band). Each satellite has a repeat cycle of 16 days, but shorter repeats may be achieved using the constellation. The shortest interferometric time period between two successive acquisitions is 1 day when using satellites CSK2 and CSK3. Figure S1 shows the CSK orbital configuration and the satellites used in this study. Here we use 1 day CSK2-CSK3 data. The SAR images are formed by concatenating 3 × CSK STRIPMAP-HIMAGE consecutive overlapping frames, each covering a 40 × 40 km swath, at 3 m resolution in both azimuth (along-track) and range (cross-track) directions. The incidence angle is 26.27° across the swath. We analyzed scenes in single-look complex (SLC) format of 67 km × 40 km in the azimuth and range directions, respectively. Polarization of the electromagnetic waves is HH (horizontal transmit and receive). Our spatiotemporal comprehensive observational scheme includes 10 images (five tandem pairs) acquired from August to December 2015 combined to produce short-term pixel offset velocity maps and double-difference interferograms highlighting potential short-term velocity changes and vertical tidal displacements, respectively.

The baseline separation between CSK2/3 is large, however, resulting in a significant sensitivity of the interferometric phase to surface topography. The height of ambiguity, or 360° variation in phase for a given change in elevation, is 16 m with a perpendicular baseline of 320 m. To detect the differential vertical motion of the glacier associated with changes in oceanic tides within one phase cycle, we therefore need to correct the interferogram from topographic residuals using a DEM with a vertical precision at the meter level (Figure S2). We use TDX data to generate such high-precision DEMs. TDX DEMs are generated from 3 m resolution SLC products provided by the German Space Agency (DLR) using the GAMMA software (Werner et al., 2000). We use TDX data acquired on 4 November 2015, which is closest in time with the CSK acquisitions. After the interferometric phase of the TDX interferograms is unwrapped (2π ambiguities removed from SAR interferograms per Goldstein et al., 1988), we use ground control points from the 2015 NASA's Land, Vegetation, and Ice Sensor (LVIS) campaign (Blair & Hofton, 2016) to estimate the absolute height, fine tune the interferometric baseline, and obtain precision, calibrated DEMs. The standard deviation of the inferred height versus LVIS height is 3.5 m (Figure S3), which quantifies the precision of our DEM.

For each CSK acquisition date, we stitch together the CSK stripmap SLCs processed by ASI and provided in a zero-doppler geometry. This step is followed by an orbit coregistration and a subsequent pixel offset assisted coregistration (Mouginot et al., 2012) to maintain phase coherence of the radar signal in fast-moving areas of the glacier. An interferogram is formed combining the registered master and slave SLCs. We apply a multilook factor of 8 in both range and azimuth directions to improve phase coherence. The TDX topographic phase is removed to produce the DInSAR interferogram.

To highlight the differential vertical deformation and grounding line position at different tidal levels, we combine the TDX data in nine DInSAR interferograms (Table 1). We coregister the multilooked interferograms using pixel offsets over nonmoving areas. By performing this step, we implicitly assume a constant horizontal ice flow during the observation period. Pixel offset velocity maps are calibrated and mosaicked together using the procedure described by Mouginot et al. (2012). Similar to Rignot et al. (2000) and Fricker et al. (2009), we

Table 1
Characteristics of the Cosmo-SkyMed (CSK) Data Acquired Over Pine Island Glacier, West Antarctica

	Master	Slave	B⊥ master (m)	B⊥ Slave (m)	Δ*h* DInSAR (m)	Δ*h* Cats2008 (m)	Bed stiffness (Gpa/m)	SW13 RMS (m)
A	2–3/8/2015	5–6/10/2015	108	124	0.55	0.27	0.83 ± 0.70	0.032
B	2–3/8/2015	21–22/10/2015	108	6	0.3	0.16	0.30 ± 0.42	0.024
C	2–3/8/2015	6–7/11/2015	108	−36	0.33	0.17	0.28 ± 0.55	0.038
D	2–3/8/2015	8–9/12/2015	108	126	0.05	0.07	-	-
E	5–6/10/2015	21–22/10/2015	124	6	−0.25	−0.11	3.40 ± 2.1	0.049
F	5–6/10/2015	6–7/11/2015	124	−36	−0.27	−0.10	0.87 ± 0.65	0.029
G	5–6/10/2015	8–9/12/2015	124	126	−0.51	−0.20	0.14 ± 0.07	0.044
H	21–22/10/2015	8–9/12/2015	6	126	−0.1	−0.09	-	
I	6–7/11/2015	8–9/12/2015	−36	126	−0.2	−0.10	0.15 ± 0.05	0.040

Note. Master is the reference CSK scene; Slave is the second scene coregistered to the master scene to produce an interferogram. We indicate the date of acquisition of the master and slave, their perpendicular baseline (B⊥), their differential tidal signal recorded in the DInSAR data, the estimate from the CATS2.01 model from the time of passage of the CSK satellites, the bed stiffness inferred from the profiles in Figure 1, and the root-mean-square error between the data and the SW13 projections along a set of profiles shown in Figure S7 (A-I).

compare the DInSAR recorded vertical differential tidal displacements with the CATS2008 tidal model (Padman et al., 2002) (Figure S4). We find a standard difference of ~5 cm, which is within the error bar of the CATS2008 model.

To track the grounding line position, we map the inward limit of detection of vertical motion, where the glacier lifts off the bed and becomes afloat, as discussed in Rignot et al. (2014). Grounding line migration is then analyzed as a function of the differential vertical tidal displacement to study the relationship between bed slope, surface slope, and grounding line position. To quantify grounding line migration, we use the elastic beam model of Sayag and Worster (2013, hereinafter SW13) that takes into account the elastic properties of an elastic deformable bed of effective stiffness k. The SW13 line model assumes an elastic ice sheet characterized by an instantaneous deformation under tidal forcing, a constant surface and bed slope, and a uniform thickness H, which is reasonable over short distances (a few kilometers or a few ice thickness). We calculate the average slope over the selected profiles using bed topography from Rignot et al. (2014) deduced from mass conservation (MC; Morlighem et al., 2011) approach that combines sparse ice thickness data collected by airborne radar sounders from (Leuschen et al., 2010) with InSAR-derived ice velocity maps (Rignot et al., 2011). Important physical parameters in the SW13 model are the bending-buoyancy length scale $l = (D/\rho_i\, g\, H)^{1/3}$ and the effective stiffness k where D, ρ_i, and g are the bending stiffness, water density, and acceleration of gravity, respectively. The distance l identifies an elastically controlled region acting as a barrier preventing leakage of subglacial melt water toward the ocean and transfer of ocean water landward. The bending stiffness k (constant in SW13) represents the resistance of the bed against the ice sheet bending deformation. Studies analyzing generation and dissipation of pore water pressure in a saturated compressible medium during dynamic loading on an alpine glacier showed that stress induced by loading depends linearly on the amount of compression (Rousselot & Fischer, 2005). The value of constrained modulus depends on the stress to which the sediment is subjected (Lambe & Whitman, 1979) and hence on the differential tidal level ΔT. In our study, we adopt $k = k_0 + \gamma\, \Delta T$. We infer k using the full coherent profiles in Figure 1b and estimate γ *by* minimizing the differences between the grounding line positions of the profiles in Figure 1a and the SW13 grounding line migration formula (equation (S11) in the supporting information) (Sayag & Worster, 2013).

To interpret the retreat pattern, we consider the ice motion pattern (Figure S6), the TDX DEM (Figure 1j), and the bed topography (Figure 1k). Thickness is obtained by subtracting the MC bed from the TDX DEM. We calculate the height above floatation as $\phi = Z_s + Z_b\ (\rho_w - \rho_i)/\rho_i$ where ρ_i is the density of ice (917 kg/m^3), ρ_w is the density of seawater (1028 kg/m^3), Z_s is the surface elevation, and Z_b is the bed elevation with respect to sea level (Figure 1l).

3. Results

Figure 1 shows the DInSAR data set together with the TDX DEM, the MC bed, and the distribution of hydrostatic potential. The variation in CSK velocity over the time period of observation—or lack thereof—is shown in Figure S5.

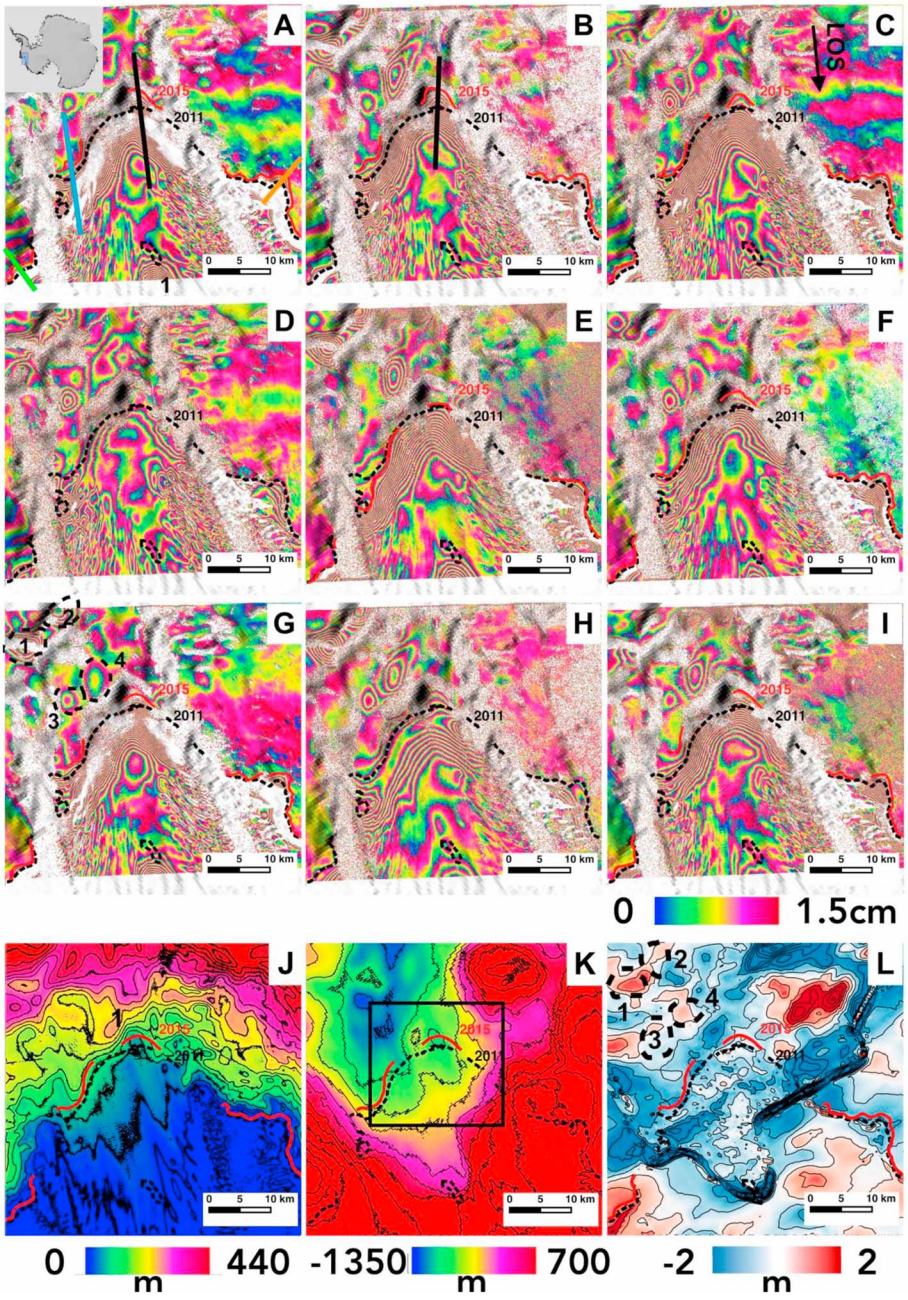

Figure 1. Tidally wrapped CSK DInSAR interferograms of Pine Island Glacier (PIG), West Antarctica. CSK is flying south, in right looking mode (line of sight, LOS, is perpendicular to the flight direction). Color tone is modulated by a shaded relief TDX DEM acquired in November 2015. Areas with no InSAR data are transparent. The 2011 grounding line position (Rignot et al., 2014) is black dashed line. (a–i) CSK DInSAR data for dates listed in Table 1; grounding line is red where detected. Thick black lines are locations of profiles in Figures 2 and S7. Locations of lakes 1–4 are shown in Figure 1g. Average grounding line position in red overlaid on (j) TDX DEM 30 m contour intervals; (k) MC bed elevation with 100 m contour intervals (Morlighem et al., 2011) and (l) along-flow hydrostatic potential with 40 cm contour interval. Black box inset is location of Figure S5.

The DInSAR reveals the vertical deformation of the ice surface at different tidal levels and the position of the grounding line. Variations in the grounding line position ranges from 0 to 4 km with reference to the 2011 grounding line position depending on the tidal level at the time of acquisition of the CSK data (Figures 1b 1e, S4b, and S4e).

Table 2
Tidally Induced Grounding Line Migration at the Pine Island Glacier, West Antarctica, as a Function of Differential Tidal Height dh

Profile	Surface slope (%)	Bed slope (%)	*H* (km)	d*h* (m)	Modeled TB78 (m)	Modeled SW13 (m)	Observed DInSAR (m)
Green	0.5	0.33	1.4	−0.5	−103.8	−810	−1126.6
				0.2	41.5	262	450.6
Black	0.9	0.5	0.85	−0.5	−58.4	−486	−635.4
				0.2	23.3	157.6	254.2
Blue	0.64	−3.5	1.2	−0.5	259.1	1462	1458
				0.2	−103.6	−474	−590
Orange	−2	−0.56	0.8	−0.5	27.11	227	119.4
				0.2	−10.84	−70	−34.1

Note. Surface and bed slopes are calculated as an average over ~2 km near the grounding zone. DInSAR values are extrapolated from trends reported in Figure 2. Profile colors refer to Figures 2 and 1A. TB78 is the migration from Thomas and Bentley (1978), SW13 is the migration from Sayag and Worster (2013) using a tidal-dependent bed stiffness, and DInSAR is the observed migration.

We compare the observed migration with the hydrostatic equilibrium model on a hard bed from Thomas and Bentley (1978, hereinafter TB78) and that calculated for an elastic, deformable bed (SW13). We select several sections of the glacier, coherent in all DInSAR data, that cross the grounding line perpendicular to the fringe rate (Figure 1b). Note that we do not study the deformation regime of ice along the shear margins where the interferometric coherence is low or absent; hence, most profiles are along the central part of the glacier. We use the interferogram vertical tidal levels and InSAR inferred bed slope, ice thickness (TDX elevation minus the MC bed elevation), and Young's modulus of ice (9.33 GPa, Hutter, 1983), and we calculate the bending-buoyancy length scale, l = 3.01 ± 0.5 km, where the error assumes a 20% uncertainty in ice thickness. These parameters are input parameters to an inversion to infer the bed stiffness from the deformation profiles. The inferred values for the bed stiffness, shown in Figure S7 and Table 1, vary between 140 ± 70 MPa/m and 3.40 ± 2.1 GPa/m. We select four coherent interferogram sections across the grounding line in the along-flow direction (Figure 1a) to study the relationship between grounding line migration and tidal cycle. These profiles are not coherent in all interferograms, but the grounding line is still visible; i.e., we cannot infer bed stiffness using SW13 but we can study the tidally induced grounding line migration. For each profile, we track the grounding line position by measuring the distance between the tidal vertical signal recorded on the ice with respect to a fixed reference upstream. We record tidally induced grounding line migrations on the order of 2 km over areas characterized by a shallow bed slope (0.5%) (Table 2 and Figure 2) and less in areas of steeper bed slope, such as the glacier center. The results indicate that tidally induced grounding line migration is proportional to the tidal vertical displacement and inversely proportional to the DEM along-flow slope. Using k_0 = 0.87 GPa/m (average bed stiffness in Table 1), we find γ = 5 ± 2.3 kPa/m^2 (Figure 2).

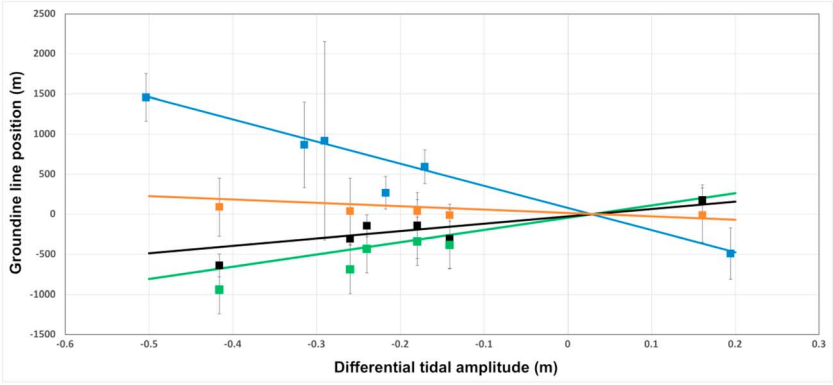

Figure 2. Tidally induced grounding line migration of Pine Island Glacier, West Antarctica, as a function of tidal height. Colors correspond to different sections in Figure 1a. Colored lines indicate tidally induced grounding line migrations using SW13 elastic bed model with ice in hydrostatic equilibrium and tidal-dependent bed stiffness. Numerical results for lines are shown in Table 2.

After characterizing the tidally induced grounding line variation and performing a model fit of the data with SW13 including a tidally dependent bed stiffness, we correct the grounding line positions for tides using the tide predictions from the CATS2008 model and compare the resulting mean sea level grounding line position to historical data positions, in particular the 2011 grounding line. More precisely, we calculate the 2015 grounding line position at the same tidal level as for the 2011 ERS-2 DInSAR derived grounding line (−0.25 m differential tidal amplitude from CATS2008 model) and measure the along-flow grounding line migration between the two different epochs. We find a 0.3 and 0.5 km/yr retreat occurring at the glacier center and closer to the sides, respectively, between 2011 and 2015 (Figures 1 and S4). If we do not correct the signal for oceanic tides, the apparent retreat rate would have been twice as large, which illustrates the importance of performing the tidal correction with an elastic bed (Figures 1b and S4b). If we compare grounding line measurements acquired at low tide with the 2011 grounding line position (i.e., Figures 1e and S4e), we would erroneously conclude that the grounding line has not retreated since 2011. With the correction, we detect a smaller rate of migration of the grounding line in 2011–2015 compared to earlier years when the grounding line was retreating about 1.2 km/yr on average (Rignot et al., 2014). Hence, the grounding line retreat slowed down in 2011–2015 compared to 1994–2011. We note here that short-term variations in grounding line position are smoothed out when considering changes over the time period 1994–2011, whereas they dominate for the change from 2011 to 2015.

On the ice shelf, we find a slightly grounded area—or ice rumple—that migrated toward the ocean by 5.8 km since 2011 (Figure 1a, point 1). We attribute the apparent migration of this ice rumple to the advection of an irregular patch of thicker ice down the glacier (Rignot et al., 2014). Similar patches of thicker ice have been observed before on PIG, for instance, on time sequences of visible imagery (Mouginot et al., 2017). The rate of migration of this feature is consistent with the glacier speed and suggests that the keel of the thick ice block interacts with the underlying bathymetry as it travels downstream.

In addition to the grounding line migration, the CSK data identify two specific anomalies in ice motion about 2.5 and 20 km upstream the grounding line, respectively (Figure 1g). The 1.5 m subsidence at positions named Lakes 1 and 2 have been interpreted as a set of subglacial lakes draining over a period of a few weeks in 2014 by Joughin et al. (2016). Our observations are obtained with the interferometric phase data instead of speckle tracking and hence are 1 order of magnitude more precise than the range offsets. They indicate that these subglacial lakes are not ephemeral but persist during the entire observational period, alternating between periods of subsidence and uplift, characterized by an amplitude of up to 10 cm. We find no detectable change in glacier speed during the apparent filling and draining of these subglacial lakes, as mentioned earlier, and the lakes appear to be permanent features fixed at the same position. We calculate the change in lake water volume from the CSK DInSAR data by summing the height change over the area where we detect vertical motion in the interferogram. We find a maximum volume of 0.15 km^3 for Lake 1 (Figure 1h) and 0.001 (Figure 1g), 0.0016, and 0.005 km^3 for Lakes 3 and 4, respectively (Figures 1g and S8). Comparing the lake location with the map of hydrostatic potential, we note that Lakes 1 and 2 are in an area of increased hydrostatic potential (Figure 1l). We note a similar increase in hydrostatic potential for Lakes 3 and 4. We find no correlation between the lake volume and the tidal level.

4. Discussion

In the past, we have had limited access to grounding line observations of this part of West Antarctica. Only six grounding line measurements have been obtained on PIG in the last 25 years using DInSAR data (Rignot et al., 2011). Grounding line mapping is challenging because of the fast glacier motion (4 km/year), which requires short repeat cycle data to avoid phase aliasing (Milillo et al., 2016; Mouginot et al., 2014; Riel et al., 2015; Rignot et al., 2014). In this study, we find that the 1 day CSK interferometric tandem pairs provide sufficiently high coherence on the fast-moving portions of the glacier to enable precision grounding line mapping over at least the center part of the glacier for the first time since 2011. The ability of acquiring multiple SAR data over short time scales is therefore a major advantage of the CSK constellation since it provides a time series of observations at a dense spatial coverage.

Between 1973 and 2010, PIG increased its ice speed by 1.7 km/yr or 75%, followed by a 0.1 km/yr slowdown between 2009 and 2013, while its flux increased from 78 ± 7 Gt/yr in 1973 to a maximum of 132 ± 4 Gt/yr in 2013, or 69% higher (Mouginot et al., 2014). During that time period, the grounding line retreated across an

ice plain or region only a few tens of meters above floatation. The grounding line is now retreating along a deep subglacial trough beneath the glacier (Rignot et al., 2014). Because the bed slope is reverse in that region, we would expect the grounding line to start retreating faster than in the past. Instead, our results indicate that the retreat rate slowed down in 2011–2015. This slowdown could be due to multiple factors. One factor is the apparent presence of a pronounced topographic feature at the glacier center, about 3 km downstream from Lake 4 (Figure 1j point 1), which is visible in both the TDX DEM and the MC bed. This topographic hill may temporarily stabilize the glacier grounding line. A second factor is the reported presence of relatively colder water in Pine Island Bay during the years 2011–2013 (Dutrieux et al., 2014) compared to earlier times. Colder water will reduce the ocean thermal forcing on the ice shelf, reducing the rate of ice shelf melt, which effectively translates into a slower rate of retreat of the glacier (Christianson et al., 2016). A recent modeling study suggests that the speed of retreat of the nearby Thwaites Glacier is strongly modulated by ocean temperature, with variations up to 30–40% between cold and warm periods (Seroussi et al., 2017).

In areas of shallow bed slope, we find that seawater flushes back and forth up to 2 km along the grounding zone. This flushing of seawater within the grounding zone has major implications. One implication is that this intrusion must fuel nonzero rates of ice melt at the mean sea level grounding line as also suggested by Horgan et al. (2013). Numerical ice sheet models typically assume zero melt at the grounding line (i.e., assume a fixed grounding line position; Favier et al., 2014). Our observations call the assumption of a fixed grounding line and zero melt into question. Further studies are needed to determine the exact intensity of ice melt within the flush zone, but it is likely not to be 0. The water column will be shallow, hence limiting the net ocean heat content that intrudes the grounding zone, but the flushing of seawater will be renewed on tidal scales, which might be sufficient enough to generate high rates of ice melt. Secondly, the tidal migration induced by the deformable bed implies that short-term monitoring of the glacier grounding line position must account for tidal effects. As noted earlier, the SW13 model including a tidally dependent bed stiffness provides a much better fit than the stiff bed model TB78 (Table 1), which suggests the presence of a soft bed beneath the PIG.

We find the same bed stiffness for all profiles (Table 1). This agreement provides confidence in the model fit and suggests that the bed properties and hydrological regime do not vary significantly across the grounding line, through time, or with the tidal cycle. A bed stiffness of 6.3 GPa/m is consistent with values derived by SW13 for the Filchner-Ronne ice shelf using satellite-based laser altimetry (Sayag & Worster, 2013). The SW13 model requires inclusion of a pressure (tide)-dependent bed stiffness to reproduce the observed grounding line migrations (Figure 2). This effect has already been observed in independent studies on alpine glaciers (Rousselot & Fischer, 2005).

The SW13 model also predicts the existence of an elastically controlled region that acts as a barrier for subglacial water melt leakage and seawater intrusion over a distance on the order of the bending-buoyancy length scale $l \sim 3$ km. Near the grounding line, the hydraulic potential is oscillatory and induces a periodic migration of the subglacial water system with the tidal cycle. Upstream, the hydrostatic potential is dominated by hydrostatic water pressure. This interpretation is compatible with our data locating subglacial Lakes 3 and 4 about 3.5 km upstream of the grounding line, which is right above the bending-buoyancy length scale.

Comparing high to low tide DInSAR measurements, we observe a 2.5 km landward shift at high tide in only one of the three available high-low tide interferograms (Figure 1b). The reason that we are not able to capture this migration might be the differential nature of our measurements since a DInSAR is formed by the difference of four images acquired at different tidal levels which may mask the migration. Our reduced amount of data at high tide (only one SAR image acquisition) does not allow us to estimate the grounding line migration at high tide. We posit that Lakes 1 and 2 exchange fresh water between each other given the in-phase alternating period of uplift and subsidence between them. We record the same behavior at Lakes 3 and 4, but the total water volume exchanged between these lakes varies more significantly. Our examination of earlier interferograms acquired in 1992, 1994, and 2000 indicates that similar lakes were present at earlier times and hence are not the result of recent changes in grounding line position or speedup on PIG but reflect a rather sustained subglacial hydrologic system (supporting information) (Rignot et al., 2014, FigS2S6_SOM 1992 (b), 1994 (b), 2000 (b)). We note that the elastic crack model of

Tsai and Gudmundsson (2015, hereinafter TG15) also provides plausible results when interpreting kilometric scale tidally induced grounding line migration. The TG15 model solves a problem of elastic crack growth viewing the interface between the ice and the bed as a horizontal fracture assuming that only elastic stresses are relevant over the 12 h time scale of interest. The crack model predicts (for high tides) a tidally induced grounding line migration for 10 times larger than the TB78 hydrostatic equilibrium model. The main limitation of TG15, however, is its applicability to the high tide regime and a prograde bed slope only, which is not the case here.

The combination of short repeat time interferometry and accurate DEM sheds new light onto the biweekly dynamics of PIG. Kilometer-scale tidally induced grounding line migration over shallow slopes are important to consider when interpreting grounding line positions acquired over short time periods. This effect is not critical over long observation periods considering a 30–35 km total retreat (Rignot et al., 2014) but becomes relevant over shorter time scales (annually to subannually).

Recent studies have neglected the tidal influence on grounding line migration and attributed it to noise (Han & Lee, 2014). A study coupling GPS measurements with InSAR data found horizontal modulation up to 60% of the tidal vertical amplitude within a few kilometers of the grounding line on the Southern McMurdo ice shelf (Rack et al., 2017). The authors hypothesized that the bending stresses were the cause of the horizontal modulation in speed. We do not find similar modulation of the flow speed extending a few kilometers upstream the grounding line on PIG and argue instead that the effect of the bending stresses is negligible and the grounding line is migrating back and forth over large distances (Figure S7). Similarly, our data set (Figure S6) does not reveal any change in ice speed (larger than 110 m/yr within our pixel offsets map sensitivity Figure S9) synchronous with oceanic tides, as in the case for another Antarctic glacier (e.g., Minchew et al. 2017). It would be of interest to further elucidate the differences in behavior of these glaciers with oceanic tides and determine how the results inform us about the fundamental basal processes taking place at the grounding line.

5. Conclusions

Using short repeat time CSK InSAR data, we characterize the short-term variability in landward extent of the grounding zone of Pine Island Glacier, in West Antarctica, shedding new light on kilometer-scale, tidally induced grounding line migration. The 1.2 km/yr retreat that prevailed in 1992–2011 has now slowed down to 0.5 km/yr in 2011–2015, which we attribute to a combination of obstruction in bed topography and reduced thermal forcing from the ocean. Our analysis reveals that kilometer-scale tidally induced grounding line migration on PIG may mask out the retreat signal on subannual scales, in excess of what is predicted for a stiff bed. We suggest that the flushing back and forth of seawater in the grounding zone should enable ice melt at the mean sea level grounding line, contrary to what numerical models generally assume, which could have an impact on modeling glacial retreat in this region. Further studies are needed to determine the amplitude of melt and its impact on the long-term glacier dynamics. The study also adds confidence in the bed mapping of the glacier using mass conservation and indicates that the subglacial lakes discussed by Joughin et al. (2016) near the grounding line of PIG are not ephemeral but permanent features with permanently changing fill levels.

Acknowledgments
This work was conducted at the Jet Propulsion Laboratory, California Institute of Technology, and at UC Irvine under a contract with the Cryosphere Program of the National Aeronautics and Space Administration. P.M. was sponsored by the National Aeronautics and Space Administration (NASA) Postdoctoral program administered by the University Space Research Association (USRA). We thank the Italian Space Agency (ASI) for providing COSMO-SkyMed data for this project (original COSMO-SkyMed product © ASI, Agenzia Spaziale Italiana (2008–2017)). We thank the German Space Agency (DLR) for providing TanDEM-X data for this project (original TanDEM-X product © DLR (2007–2017)). TanDEM-X CoSSC data for this project were provided by the German Aerospace Center (DLR) under proposal NTI_INSA7085. Displacement fields and other processed SAR data are available from the authors upon request.

References

Blair, J. B., & Hofton, M. (2016). *IceBridge LVIS L1B Geolocated Return Energy Waveforms, Version 2*. [Indicate subset used]. Boulder, CO: NASA National Snow and Ice Data Center Distributed Active Archive Center. https://doi.org/10.5067/RDT1MZVS0VG9

Christianson, K., Bushuk, M., Dutrieux, P., Parizek, B. R., Joughin, I. R., Alley, R. B., … Holland, D. M. (2016). Sensitivity of Pine Island Glacier to observed ocean forcing. *Geophysical Research Letters*, *43*, 10,817–10,825. https://doi.org/10.1002/2016GL070500

Dutrieux, P., De Rydt, J., Jenkins, A., Holland, P. R., Ha, H. K., Lee, S. H., … Schröder, M. (2014). Strong sensitivity of Pine Island ice-shelf melting to climatic variability. *Science*, *343*(6167), 174–178. https://doi.org/10.1126/science.1244341

Favier, L., Durand, G., Cornford, S. L., Gudmundsson, G. H., Gagliardini, O., Gillet-Chaulet, F., … Le Brocq, A. M. (2014). Retreat of Pine Island Glacier controlled by marine ice-sheet instability. *Nature Climate Change*, *4*, 117–121. https://doi.org/10.1038/nclimate2094

Fricker, H. A., Coleman, R., Padman, L., Scambos, T. A., Bohlander, J., & Brunt, K. M. (2009). Mapping the grounding zone of the Amery Ice Shelf, East Antarctica using InSAR. *MODIS and ICESat, Antarctic Science*, *21*(5), 515–532. https://doi.org/10.1017/S095410200999023X

Goldstein, R. M., Zebker, H. A., & Werner, C. L. (1988). Satellite radar interferometry: Two-dimensional phase unwrapping. *Radio Science*, *23*(4), 713–720. https://doi.org/10.1029/RS023i004p00713

Han, H., & Lee, H. (2014). Tide deflection of Campbell Glacier Tongue, Antarctica, analyzed by double-differential SAR interferometry and finite element method. *Remote Sensing of Environment*, *141*, 201–213.

Han, H., Im, J., & Kim, H. C. (2016). Variations in ice velocities of Pine Island Glacier Ice Shelf evaluated using multispectral image matching of Landsat time series data. *Remote Sensing of Environment*, *186*, 358–371.
Horgan, H. J., Alley, R. B., Christianson, K., Jacobel, R. W., Anandakrishnan, S., Muto, A., … Siegfried, M. R. (2013). Estuaries beneath ice sheets. *Geology*, *41*(11), 1159–1162. https://doi.org/10.1130/G34654.1
Hutter, K. (1983). *Theoretical Glaciology*. Norwell, Mass: D. Reidel.
Jenkins, A. (2016). A simple model of the ice shelf-ocean boundary layer and current. *Journal of Physical Oceanography*, *46*(6), 1785–1803. https://doi.org/10.1175/JPO-D-15-0194.1
Joughin, I., Shean, D. E., Smith, B. E., & Dutrieux, P. (2016). Grounding line variability and subglacial lake drainage on Pine Island Glacier, Antarctica. *Geophysical Research Letters*, *43*, 9093–9102. https://doi.org/10.1002/2016GL070259
Lambe, T. W., & Whitman, R. V. (1979). *Soil Mechanics*, SI Version. Hoboken, NJ: John Wiley.
Leuschen, C., Gogineni, P., Rodriguez-Morales, F., Paden, J., & Allen, C. (2010). *IceBridge MCoRDS L2 ice thickness*, Version 1. Boulder, CO: NASA National Snow and Ice Data Center Distributed Active Archive Center.
Milillo, P., Riel, B., Minchew, B., Yun, S. H., Simons, M., & Lundgren, P. (2016). On the synergistic use of SAR constellations' data exploitation for Earth science and natural hazard response. *IEEE Journal of Selected Topics in Applied Earth Observations and Remote Sensing*, *9*(3), 1095–1100.
Minchew, B. M., Simons, M., Riel, B., & Milillo, P. (2017). Tidally induced variations in vertical and horizontal motion on Rutford Ice Stream, West Antarctica, inferred from remotely sensed observations. *Journal of Geophysical Research: Earth Surface*, *122*, 167–190. https://doi.org/10.1002/2016JF003971
Morlighem, M., Rignot, E., Seroussi, H., Larour, E., Ben Dhia, H., & Aubry, D. (2011). A mass conservation approach for mapping glacier ice thickness. *Geophysical Research Letters*, *38*, L19503. https://doi.org/10.1029/2011GL048659
Mouginot, J., Scheuchl, B., & Rignot, E. (2012). Mapping of ice motion in Antarctica using synthetic-aperture radar data. *Remote Sensing*, *4*(9), 2753–2767. https://doi.org/10.3390/rs4092753
Mouginot, J., Rignot, E., & Scheuchl, B. (2014). Sustained increase in ice discharge from the Amundsen Sea embayment, West Antarctica, from 1973 to 2013. *Geophysical Research Letters*, *41*, 1576–1584. https://doi.org/10.1002/2013GL059069
Mouginot, J., Rignot, E., Scheuchl, B., & Millan, R. (2017). Comprehensive annual ice sheet velocity mapping using Landsat-8, Sentinel-1, and RADARSAT-2 data. *Remote Sensing*, *9*(4), 364.
Padman, L., Fricker, H. A., Coleman, R., Howard, S., & Erofeeva, S. (2002). A new tidal model for the Antarctic ice shelves and seas. *Annals of Glaciology*, *34*, 247–254. https://doi.org/10.3189/172756402781817752
Park, J., Gourmelen, N., Shepherd, A., Kim, S., Vaughan, D., & Wingham, D. (2013). Sustained retreat of Pine Island Glacier. *Geophysical Research Letters*, *40*, 2137–2142. https://doi.org/10.1002/grl.50379
Rack, W., King, M. A., Marsh, O. J., Wild, C. T., & Floricioiu, D. (2017). Analysis of ice shelf flexure and its InSAR representation in the grounding zone of the Southern McMurdo Ice Shelf, *The Cryosphere Discussions*. https://doi.org/10.5194/tc-2017-13
Riel, B., Milillo, P., Simons, M., Lundgren, P., Kanamori, H., & Samsonov, S. (2015). The collapse of Bárðarbunga Caldera, Iceland. *Geophysical Journal International*, *202*(1), 446–453. https://doi.org/10.1093/gji/ggv157
Rignot, E. (2008). Changes in West Antarctic ice stream dynamics observed with ALOS PALSAR data. *Geophysical Research Letters*, *35*, L12505. https://doi.org/10.1029/2008GL033365
Rignot, E., Padman, L., MacAyeal, D. R., & Schmeltz, M. (2000). Observation of ocean tides below the Filchner and Ronne ice shelves, Antarctica, using synthetic aperture radar interferometry: Comparison with tide model predictions. *Journal of Geophysical Research*, *105*(C8), 19,615–19,630. https://doi.org/10.1029/1999JC000011
Rignot, E., Bamber, J. L., van den Broeke, M. R., Davis, C., Li, Y., van de Berg, W. J., & van Meijgaard, E. (2008). Recent Antarctic ice mass loss from radar interferometry and regional climate modelling. *Nature Geoscience*, *1*, 106–110. https://doi.org/10.1038/ngeo102
Rignot, E., Mouginot, J., & Scheuchl, B. (2011). Antarctic grounding line mapping from differential satellite radar interferometry. *Geophysical Research Letters*, *38*, L10504. https://doi.org/10.1029/2011GL047109
Rignot, E., Mouginot, J., Morlighem, M., Seroussi, H., & Scheuchl, B. (2014). Widespread, rapid grounding line retreat of Pine Island, Thwaites, Smith, and Kohler Glaciers, West Antarctica, from 1992 to 2011. *Geophysical Research Letters*, *41*, 3502–3509. https://doi.org/10.1002/2014GL060140
Rignot, E. J. (1998). Fast recession of a West Antarctic glacier. *Science*, *281*(5376), 549–551. https://doi.org/10.1126/science.281.5376.549
Rousselot, M., & Fischer, U. H. (2005). Evidence for excess pore-water pressure generated in subglacial sediment: Implications for clast ploughing. *Geophysical Research Letters*, *32*, L11501. https://doi.org/10.1029/2005GL022642
Sayag, R., & Worster, M. G. (2013). Elastic dynamics and tidal migration of grounding lines modify subglacial lubrication and melting. *Geophysical Research Letters*, *40*, 5877–5881. https://doi.org/10.1002/2013GL057942
Scheuchl, B., Mouginot, J., Rignot, E., Morlighem, M., & Khazendar, A. (2016). Grounding line retreat of Pope, Smith, and Kohler Glaciers, West Antarctica, measured with Sentinel-1a radar interferometry data. *Geophysical Research Letters*, *43*, 8572–8579. https://doi.org/10.1002/2016GL069287
Seroussi, H., Nakayama, Y., Larour, E., Menemenlis, D., Morlighem, M., Rignot, E., & Khazendar, A. (2017). Continued retreat of Thwaites Glacier, West Antarctica, controlled by bed topography and ocean circulation. *Geophysical Research Letters*, *44*, 6191–6199. https://doi.org/10.1002/2017GL072910
Shepherd A., & Peacock, N. R. (2003). Ice shelf tidal motion derived from ERS altimetry. *Journal of Geophysical Research*, *108*(C6), 3198. https://doi.org/10.1029/2001JC001152
Shepherd, A., Wingham, D. J., Mansley, J. A. D., & Corr, H. F. J. (2001). Inland thinning of Pine Island Glacier, West Antarctica. *Science*, *291*(5505), 862. https://doi.org/10.1126/science.291.5505.862
Shepherd, A., Wingham, D. J., & Mansley, J. A. D. (2002). Inland thinning of Amundsen Sea sector, West Antarctica, *Geophysical Research Letters*, *29*(10), 1364. https://doi.org/10.1029/2001GL014183
Thomas, R. H., & Bentley, C. R. (1978). A model for Holocene retreat of the West Antarctic Ice Sheet. *Quaternary Research*, *10*(2), 150–170.
Tsai, V. C., & Gudmundsson, G. H. (2015). An improved model for tidally modulated grounding-line migration. *Journal of Glaciology*, *61*(226), 216–222.
Werner, C., Wegmüller, U., Strozzi, T., & Wiesmann, A. (2000). Gamma SAR and interferometric processing software. In Proceedings of the ERS-ENVISAT Symposium, Gothenburg, Sweden. https://www.gamma-rs.ch/uploads/media/2000-1_GAMMA_Software.pdf